2026-01-5024 Published 30 Mar 2026

Analyzing Effects of Cell to Chassis Technology on Sound Transmission Loss of Skateboard- Sharing Vehicles

Xueying Xu CATL

Xiaoming Wang, Caijun Ma, and Guofu Li Institute of Acoustics

Citation: Xu, X., Wang, X., Ma, C., and Li, G., "Analyzing Effects of Cell to Chassis Technology on Sound Transmission Loss of Skateboard- Sharing Vehicles," SAE Technical Paper 2026-01-5024, 2026, doi:10.4271/2026-01-5024.

Received: 06 Nov 2025 Revised: 06 Jan 2026 Accepted: 09 Mar 2026

Abstract

Limited published research has critically examined the impact of Cell-to-Chassis (CTC) structures on the Noise, Vibration, and Harshness (NVH) performance of electric vehicles (EVs), with most studies focusing on conventional Cell-to-Pack (CTP) systems. A concern is that vehicles employing CTC architectures may exhibit compromised NVH performance due to the absence of a dedicated floor panel. To investigate the NVH performance implications of the CTC structure, this study adopts a comprehensive methodology encompassing: (1) theoretical Sound Transmission Loss (STL) analysis utilizing mass law and double-panel principles, (2) finite element (FE) modeling of STL, (3) in-vehicle Acoustic Transfer Function (ATF) testing, and (4) interior noise measurements conducted at a constant 60 km/h on a smooth asphalt road. Simulation results demonstrate that, compared to a conventional CTP floor system, the studied CTC structure achieves a 5–40 dB increase in STL across the 200–2000 Hz frequency range. This finding is consistent with theoretical calculations. Furthermore, experimental results from in-vehicle ATF and interior noise tests reveal no significant acoustic difference in the 400–1400 Hz frequency range, which is primarily associated with tire noise, between a configuration with complete floor insulation (including carpeting) and one with insulation (including carpeting) removed from the CTC area. This research validates an effective simulation method for floor system STL and demonstrates that the acoustic insulation performance of the CTC structure enables potential cost and weight reductions by minimizing the requirement for traditional carpeting and sound insulation pads. This approach also suggests a pathway to reducing Volatile Organic Compound (VOC) emissions from these ancillary materials.

Keywords

NVH, Sound Transmission Loss, Tire noise, Mass law, Cell to chassis, Electric vehicle

Introduction

The global shift to vehicle electrification, with sales surging 35% in 2023 [1], is reshaping automotive NVH. In EVs, the absence of engine masking amplifies high-frequency sounds like tire and road noise, making body acoustic performance critical for cabin comfort [2]. This, combined with persistent consumer range anxiety, has driven a two-pronged evolution in lightweight design. First, the heavy battery system (up to 500 kg) has evolved from Module-to-Pack (MTP) to integrated CTP solutions, enhancing energy density and structural contribution [3, 4]. Second, traditional heavy mass-barrier sound packages [5] are being replaced by lightweight alternatives like single-layer porous absorbers [6, 7]. These concurrent changes—a stiffer integrated floor from below and a lighter acoustic package from above—alter both low-frequency structural dynamics and high-frequency sound transmission [8], mandating a full re-evaluation of the floor-carpet system to manage road noise.

The latest frontier is the CTC and Cell-to-Body (CTB) concept, where the battery's top cover serves as the vehicle

floor. This represents a fundamental shift from CTP, which, as a bolt-on component, introduces flanking paths. These paths, created by incomplete sealing, allow noise to bypass the CTP pack itself, undermining its mass-barrier advantage before the sound even reaches the main floor system [8]. In contrast, CTC achieves a monolithic fusion of energy and structural systems. Despite its revolutionary nature, research on the NVH implications of CTC/CTB is scarce. Existing literature focuses on CTP's benefits as a mass barrier [9] or its contribution to stiffness [10]. While the few available studies report dramatic structural gains—such as global stiffness increases exceeding 50% with CTB [11] and local dynamic stiffness increases by 20 times in the 20–300 Hz frequency range with CTC [12]—they do not analyze the airborne noise benefit of this structure. Consequently, the acoustic transmission loss (STL) of the CTC structure is a critical unknown. Understanding this property is crucial to properly engineer the floor's acoustic treatment, avoiding the risks of over-design (adding cost and weight) or under-design (compromising cabin comfort) [13].

This raises a critical research question: By eliminating the dedicated vehicle floor, will a CTC structure exhibit inferior airborne sound insulation compared to a conventional floor-CTP system, despite its significant structural advantages? This paper is structured to answer this question and thus fill this knowledge gap. First, a theoretical comparison (i.e., analytical solutions from classical formulas) of STL is conducted for three configurations (a single-layer floor, a floor-CTP system, and a CTC structure). Next, FE models of these configurations are developed to simulate (i.e., numerical solutions via Finite Element Analysis) STL, incorporating key structural and acoustic parameters such as Young's modulus, Poisson's ratio, density, and damping factor. Finally, an experimental validation is performed using in-vehicle Acoustic Transfer Function (ATF) and interior noise measurements to experimentally validate the superior STL of the CTC structure. The remainder of this paper details the methodologies, presents the comparative results, and discusses the implications of CTC technology for vehicle NVH design.

Literature Review

STL of Traditional Automotive Floor Systems

The vehicle floor is a primary pathway for noise into the cabin, and predicting its STL has been a central focus of automotive NVH research. In the era of internal combustion engine (ICE) vehicles, the floor panel has been predominantly modeled as a thin, single-layer metallic plate, often reinforced with structural cross-members [14, 15]. The acoustic behavior of such panels is well-understood. In the non-resonant frequency range, its STL is primarily controlled by the mass law [16]. However, in the resonant range, the STL is dictated by the panel's structural modes and their radiation efficiency, characterized by significant dips in the STL curve, particularly at the critical coincidence frequency [17, 18]. Numerous studies have shown that increasing structural damping is an effective method to mitigate these resonant dips and improve overall STL [19].

To address the complexity of real-world floor panels, advanced modeling techniques have been developed. Wang [15] employed a hybrid FEA-SEA method to study a floor panel with integrated cross-members, quantifying the significant impact of structural damping and access holes on STL. Analytical and numerical methods for predicting the STL of various plate constructions are now mature, as comprehensively summarized in several review articles [20, 21], providing a robust foundation for analyzing traditional automotive structures.

Emerging Challenges with Integrated Battery Packs in EVs

The advent of CTP battery systems in EVs fundamentally alters the floor's acoustic paradigm, transforming it into a double-wall construction: the vehicle floor panel, an air cavity, and the battery pack's top cover. The behavior of double-wall structures is more complex, featuring a mass-air-mass resonance that creates a pronounced STL dip at a low frequency [17]. The characteristics of the air cavity—its thickness and any absorptive material within—play a crucial role in the overall STL performance [22–24]. Recent research has begun to tackle this. Brentnall et al. [8] successfully used SEA and FEM to model this double-wall system, demonstrating its potential acoustic benefits. However, a critical real-world complication is the imperfect connection between the CTP pack and the body. These sealing imperfections create flanking paths, allowing sound to bypass the main structure and severely degrade the theoretically achievable STL [25, 26].

Most recently, the CTC architecture represents another leap in integration. It creates not a double-wall, but a thick, highly stiffened, single-layer composite structure. Its acoustic behavior remains largely uncharacterized. To date, a comprehensive literature search reveals a lack of studies specifically investigating the STL of these novel CTC structures. This research gap presents a significant challenge for NVH engineers. Therefore, developing a reliable and efficient method—from simple analytical models to detailed simulations—to characterize the STL of CTC structure is a pressing and critical need for the future of EV lightweighting and NVH design [2].

Structural Configuration and Component Simplification

To study the effect of the CTC structure on the airborne noise of skateboard-sharing vehicles, the actual structure is inevitably simplified. In addition, three configurations are presented: the CTC structure and two conventional floor configurations—the single-layer floor for ICE vehicles, and the CTP floor structure for EVs.

FIGURE 1 Schematic cross sections of vehicle with different floor configurations.

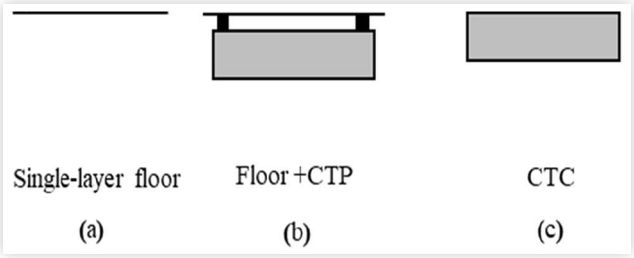

Conventional Single-Layer Floor (ICE Vehicles): This represents a simplified floor panel found in traditional ICE vehicles, acting as a primary structural element without a battery pack. For modeling purposes, this is represented by a 1-mm-thick flat steel panel, as shown in Figure 1(a).

CTP Battery System (EVs): This configuration consists of a conventional single-layer floor panel and a CTP battery pack, which is mounted to the vehicle body frame through bolts along its sides, while the center area of the floor panel is partially supported by the CTP through several bolts in the vertical direction. A significant air gap (8–10 mm) typically exists between the battery's top cover and the vehicle floor. This air gap is normally sealed with porous material to reduce the potential acoustic flanking path. For simplification in the theoretical analysis of STL, the floor panel is modeled as a 1-mm-thick steel flat plate, the CTP battery pack with inner complex batteries as a 150-mm-thick limp and isotropic component with a mass of 500 kg, and the bolts between them are omitted, as shown in Figure 1(b).

CTC Architecture (Skateboard-Sharing Vehicles): This novel design integrates battery cells directly with the battery's cover. In this configuration, the flat bottom of the battery cells is adhesively bonded to the battery's cover, which also serves as the vehicle floor panel. The electrochemical components (e.g., positive and negative terminals, pressure relief valve) are oriented downward. Furthermore, the internal structure of the battery cell—comprising a cathode, an anode, a separator, and an electrolyte—is complex, orthotropic, and layered. When many prismatic cells are joined through side connections and tightly bonded to the cover panel, this integration forms a single, unified and relatively rigid structure. For theoretical analysis, the entire CTC structure—including the floor panel, cells, and bottom plate—is simplified to a 150-mm-thick limp and isotropic component with a mass of 500 kg, as shown in Figure 1(c).

Airborne Noise Analysis

The underbody structures of the three configurations are structurally distinct. The conventional ICE vehicle features a thin, single-layer panel, whereas the CTP system includes a separate battery pack attached to the vehicle body. In contrast, the CTC architecture is a single, 150 mm-thick monolithic structure. These fundamental differences imply significant variations in their airborne noise STL, warranting an in-depth study. Such an analysis is crucial for optimizing NVH performance of skateboard-sharing vehicles by balancing cost, mass, and acoustic targets, thereby avoiding both over- and under-engineering.

Theoretical Analysis: STL

The STL of walls is governed by stiffness, mass, and damping properties [27]. Simple formulae for the STL of single and double walls are presented by Bies [28]. Assuming the single wall is limp and isotropic, and considering the frequency range of interest for this study (e.g., between the first resonance and half of the critical frequency), the STL of a single wall is given by Equation 1 [28]:

$$\mathrm{TL} = 20\log_{10}\left(\frac{\pi f m}{\rho c}\right) - 5.5 \tag{1}$$

where TL is the field incidence transmission loss with the assumption that $fm/\rho c > 1$, expressed in decibels (dB), m is the mass per unit area (kg/m²), f is frequency (Hz), ρ is the density of air (kg/m³), and c is the speed of sound in air (m/s).

The mass law is suitable for calculating the STL of single-layer floors and CTC structures. However, the floor-CTP system is relatively complicated. As shown in Figure 1(b), the region occupied by CTP accounts for 90% of the total floor area, and a porous material, approximately 20 mm wide and 10 mm high, is adhered to the CTP top cover along the sides, acting as a sealant. From an acoustic perspective, this CTP-air-floor structure can be treated as a double-wall system, which is more efficient than single-layer systems in terms of STL.

For double-wall constructions where two panels are completely isolated both mechanically and acoustically, the expected STL is given by the following equations [28]:

$$\mathrm{TL} = \mathrm{TL}_1 + \mathrm{TL}_2 + 20\log_{10} fd - 29, \quad f_0 < f < f_I \tag{2}$$

$$f_0 = \frac{1}{2\pi}\sqrt{\frac{1.8\rho c^2\left(m_1 + m_2\right)}{d m_1 m_2}} \tag{3}$$

$$f_I = \frac{c}{2\pi d} = \frac{55}{d} \tag{4}$$

where TL_1, TL_2 are the STL of the individual panels, calculated using Equation 1 with their respective surface densities m_1 and m_2. The term d represents the depth of the air gap between the panels, f_0 is the mass-air-mass resonance frequency, f_I is the limiting frequency related to the air gap width d.

Equation 2 is formulated on the assumption that standing waves and the lowest order cavity resonance in the air gap between the two panels are prevented, so that airborne coupling is negligible. Given that the air gap is only 10 mm and the surface density of the CTP is substantially higher than that of the floor panel, it can be assumed that this condition is met and airborne decoupling is effectively achieved.

The floor-CTP system consists of double-wall and single-wall regions, each characterized by a different transmission coefficient. The STL of the composite system is determined as an overall area-weighted average of both. For this calculation, Equation 5 is used [28]:

$$\tau = \frac{S_1\tau_1 + S_2\tau_2}{S_1 + S_2} \quad (5)$$

In Equation 5, S_1 is the surface area (m²) of the floor region not covered by the CTP, and τ_1 is the corresponding transmission coefficient (dimensionless) for this single-wall region. Similarly, S_2 is the surface area (m²) of the floor covered by the CTP, and τ_2 is the transmission coefficient (dimensionless) of this double-wall system.

The transmission coefficient of any element may be calculated from its Transmission Loss using the following relationship [28]:

$$\tau = 10^{\left(-\frac{TL}{10}\right)} \quad (6)$$

The overall transmission coefficient is calculated using Equation 5, from which the total TL is subsequently determined using Equation 7 [28].

$$TL = -10\log_{10}\tau \quad (7)$$

Table 1 provides a detailed breakdown of the configuration parameters for each kind of floor system. The CTP EV-floor and ICE floor are considered identical for this analysis. This is a reasonable engineering simplification, as the minor physical differences in mass and geometry result in a theoretically negligible variation in STL (i.e., less than 0.5 dB) within the mid- to high-frequency range of interest, and thus do not affect the comparative conclusions of the study.

Figure 2 compares the STL of the single-layer ICE floor, the floor-CTP system, and the CTC structure. The CTC structure provides the best acoustic insulation, outperforming the floor-CTP system by approximately 15 dB. The single-layer ICE floor is the least effective, with an STL roughly 10 dB lower than the floor-CTP system. Although its single-wall section accounts for only 10% of the total area, the parallel nature of the curves suggests the floor-CTP system's performance is dominated by the mass-law behavior of this section—a trend that governs the single-layer and CTC structures as well.

TABLE 1 Physical parameters of the three different floor configurations.

Configuration	$L \times W \times H$ (m³)	Weight (kg)	Note
ICE floor	2.5 × 1.5 × 0.001	29.25	
CTP EV-Floor	2.5 × 1.5 × 0.001	29.25	Bolts omitted
CTP EV-CTP	2.375 × 1.425 × 0.15	500	With sealant
EV CTC	2.5 × 1.5 × 0.15	500	

FIGURE 2 TL of three different floor structures based on theoretical calculation.

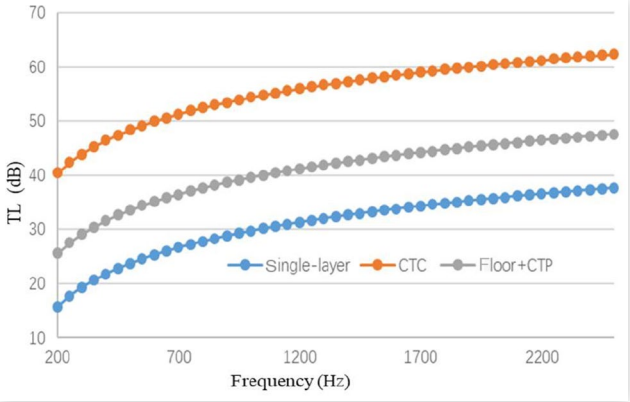

A theoretical analysis of the floor-CTP system was conducted using a double-wall acoustic model. Applying the principles outlined in Equations 3 and 4 with the component parameters from Table 1, the model yields a fundamental mass-air-mass resonance frequency (f_0) of 293 Hz. Below this critical frequency, the two panels tend to move in phase, negating the double-wall insulation effect. Meanwhile, the same analysis yields an air cavity limiting frequency (f_l) of 5500 Hz. This value is well beyond the primary frequency range of concern for vehicle interior noise, confirming the model's applicability across our frequencies of interest.

It is crucial to acknowledge that this theoretical calculation relies on highly idealized assumptions, including perfect panel decoupling, the omission of structural sound bridges (like bolts), and an absence of coincidence effects. As these ideal conditions are not met in a real-world assembly, the measured STL is expected to be lower than the theoretical value. The calculated curve should therefore be interpreted not as an exact prediction, but as an optimistic upper bound on the system's performance.

A key finding is that the floor-CTP system, despite being structurally more complex, provides inferior acoustic insulation compared to the CTC structure. This underperformance is attributed to its composite design, which incorporates both acoustically strong double-wall sections and weaker single-wall sections. As defined by the area-weighted average in Equation 5, the overall STL is disproportionately degraded by these single-wall regions.

To test this hypothesis, we simulated an idealized floor-CTP system with all single-wall areas removed. The results, plotted in Figure 3, reveal a dramatic performance increase. The STL of this idealized system not only improves but even exceeds that of the CTC structure at frequencies above 300 Hz. The curve's shape also transforms, exhibiting the classic double-wall behavior: poor performance below a resonance frequency (~300 Hz) followed by a rapid increase in STL. This finding confirms that a significant, yet untapped, acoustic potential exists within the current floor-CTP architecture. Harnessing this potential, however, hinges critically on achieving effective acoustic sealing between the CTP and the body frame.

FIGURE 3 TL of the floor-CTP system (100% double wall) and other two floor configurations.

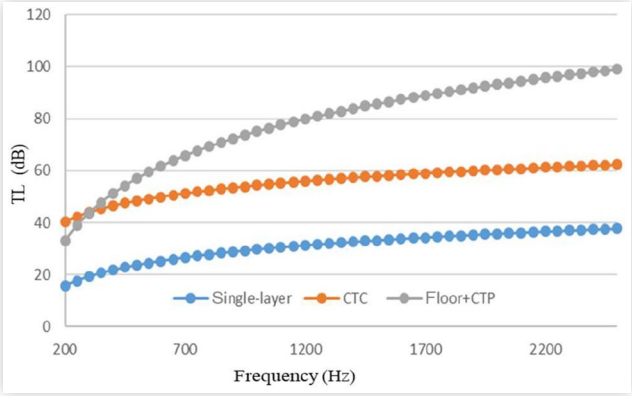

FE Simulation of STL

To obtain a more nuanced, frequency-dependent understanding, the STL of the three floor systems was simulated using Siemens Simcenter 3D software. The corresponding FE models are depicted in Figure 4.

The simulation methodology is illustrated in Figure 4. Models for the single-layer ICE floor (a), floor-CTP system (b), and CTC structure (c) were defined with rigidly clamped boundary conditions. Each structure was subjected to a diffuse acoustic field, excited by a distributed plane wave source applied to its exterior surface (blue region), Transmission Loss was calculated as the ratio of incident to transmitted acoustic power into a receiving cavity, with an Automatically Matched Layer (AML) applied to the outer boundary (green region) to absorb outgoing waves and prevent reflection. The formal definition for TL follows Equation 8 [28]:

$$TL = 10\log_{10}\frac{|P_i|}{|P_t|} \tag{8}$$

where P_i (W) and P_t (W) represent the incident and transmitted acoustic powers, respectively.

FIGURE 4 FE models of three different floor configurations.

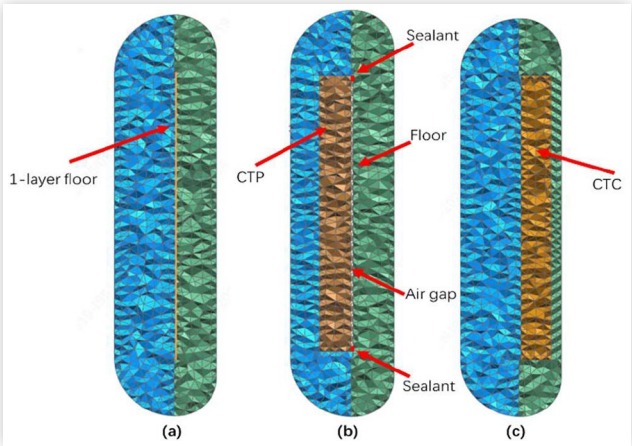

TABLE 2 Physical parameters of the three different floor systems in FE Model.

Configuration	Young's modulus (GPa)	Density (kg/m³)	Poisson's ratio	Damping coefficient
ICE floor	207	7829	0.29	0.04
CTP EV-floor	207	7829	0.29	0.04
CTP EV-CTP	70	985	0.33	0.04
EV CTC	70	889	0.33	0.04

Table 2 presents the physical parameters used for the three models. To ensure consistency in comparison, the physical parameters for CTP and CTC structures were assumed to be identical. Due to their complex internal geometries, both structures were simplified and modeled as homogeneous, isotropic materials. Their masses are treated as equivalent values. For stiffness, the Young's modulus of aluminum was used as a representative value, given its common use in structural components. A Poisson's ratio of 0.33 and a damping ratio of 0.04 were uniformly applied. As for the geometric parameters, they were kept the same as previously mentioned. While these material and geometric simplifications will inevitably affect the absolute values of resonant frequencies and STL amplitudes, they do not compromise the study's primary objective. Since these assumptions are applied consistently across all models, they provide a valid basis for comparative A-B analysis and for predicting performance trends.

As shown in Figure 5, the simulated STL curves show good qualitative agreement with the general trends from the theoretical analysis in Figure 2. The CTC structure consistently provides the highest sound insulation across the entire frequency range, while the single-layer ICE floor offers the lowest, aligning closely with mass-law predictions. The floor-CTP system's performance falls between these two benchmarks. However, a key difference from the idealized theoretical curves is the presence of distinct performance dips. The STL curve for the CTC structure exhibits prominent valleys at 750 Hz, 1000 Hz, and 1700 Hz, and the floor-CTP system displays significant

FIGURE 5 TL results for three floor configurations based on the FE Model.

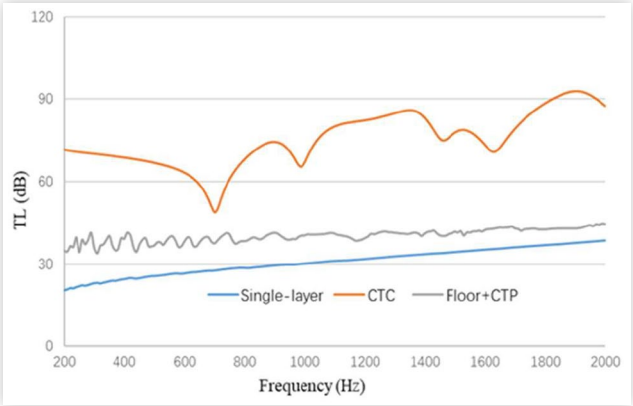

fluctuations, causing both to deviate from a simple +6 dB/octave mass-law slope. In contrast, the single-layer ICE floor's curve remains relatively smooth.

These behaviors stem from the higher fidelity of the simulation model, which incorporates factors neglected in the initial theoretical analysis. The performance dips in the CTC and floor-CTP curves are caused by the inclusion of panel stiffness, which allows structural modes to be excited at specific resonance frequencies. For the floor-CTP system, the analysis is further complicated by the coupling between the structural modes of the panels and the cavity modes of the air gap, leading to its highly fluctuating STL. The smoothness of the single-layer floor's curve is attributed to its simple, flat geometry and included damping, which creates a high density of overlapping modes that average out any distinct resonances. In summary, the simulation's use of a diffuse sound field, clamped boundaries, stiffness, damping, and air-structure coupling provides a more realistic, albeit lower, STL prediction than the idealized model. Crucially, the simulation reinforces that the floor-CTP system's performance is substantially limited by its single-wall regions, causing its STL to closely track that of the basic single-layer floor. In contrast, the CTC structure leverages its inherent mass advantage to achieve a consistently higher STL, highlighting it as the superior design.

In-Vehicle Experiment: ATF

ATF is defined as the frequency-dependent ratio of the sound pressure (Pa) at a response point to the volume acceleration (m^3/s^2) of a source. It is a key metric used to characterize airborne noise paths within a vehicle. The ATF is typically expressed in decibels (dB) as the ATF in Level (ATFL). This is calculated relative to a standard reference of 20 $\mu Pa/m^3/s^2$. To ensure a valid measurement, the ATF should be measured using a uniform acoustic point source [29].

$$\mathrm{ATF} = \frac{p}{Q_a} \tag{9}$$

$$\mathrm{ATFL} = 20\log_{10}\left(\left|\frac{p}{Q_a}\right|\right) + 94 \tag{10}$$

where $|p/Q_a|$ is the ATF amplitude of the response pressure to the volume acceleration and p/Q_a is the 1/3 octave band spectra converted from the narrow band ATF.

An ATF-based method is used to evaluate the in-vehicle STL of the CTC structure. Direct measurement is impractical because the CTC's high STL (Figure 2) is masked by flanking paths like the firewall and door panels. The approach involves measuring the ATF from a tire noise source to the cabin with and without the overlying carpet and insulation pad. A negligible difference would confirm the CTC's intrinsic STL is sufficiently high.

Figure 6 illustrates the experimental setup. It shows the carpet and sound insulation pad with areas marked for cutting (in red), along with the measurement positions for source volume acceleration at the tire and response pressure in the cabin. To simulate tire noise, acoustic point sources are positioned near the tire-road contact area, and microphones are mounted at the passenger's ear position. The test involves two scenarios: one with the carpet and sound insulation pad installed, and another with these materials removed.

FIGURE 6 Schematic of ATF measuring points and carpet pad.

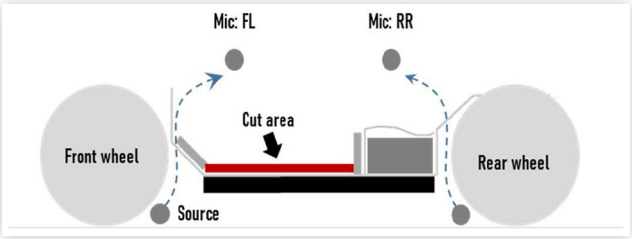

Figure 7 shows the structure of the floor system. The insulation pad comprises a porous material and a heavy layer. Together with the floor panel (in this case, the CTC structure), these form a double-wall system that provides high acoustic insulation. Tufted and flocked carpets are two common types. They primarily serve the function of sound absorption, decoration, and foot support. The surface absorption of the carpet is also beneficial for reducing interior noise, especially at middle and high frequencies, thus helping to mitigate wind noise and Electric Drive Unit (EDU) noise of EVs.

Figure 8 shows sections of the carpet and insulation pad removed from the foot wells, indicated by red lines. ATF tests compared a baseline (full insulation) with a "cut" version (sections removed). Microphones at the driver's and rear passenger's ears served as receivers, while the four tires acted as point sources. Of the eight resulting transmission paths, this analysis focuses on the four most significant: front tires to front passenger and rear tires to rear passenger.

To quantify the difference brought by the cut carpet system, the ATF under two conditions was measured

FIGURE 7 Schematic of floor system based on CTC structure.

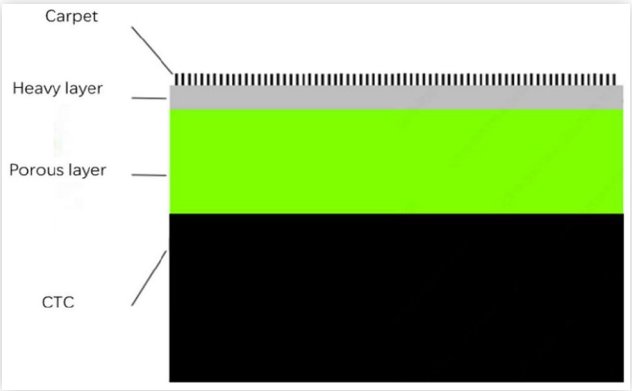

FIGURE 8 Views of the cut carpet and sound insulation pad in the vehicle: (a) first-row seat; (b) second-row seat.

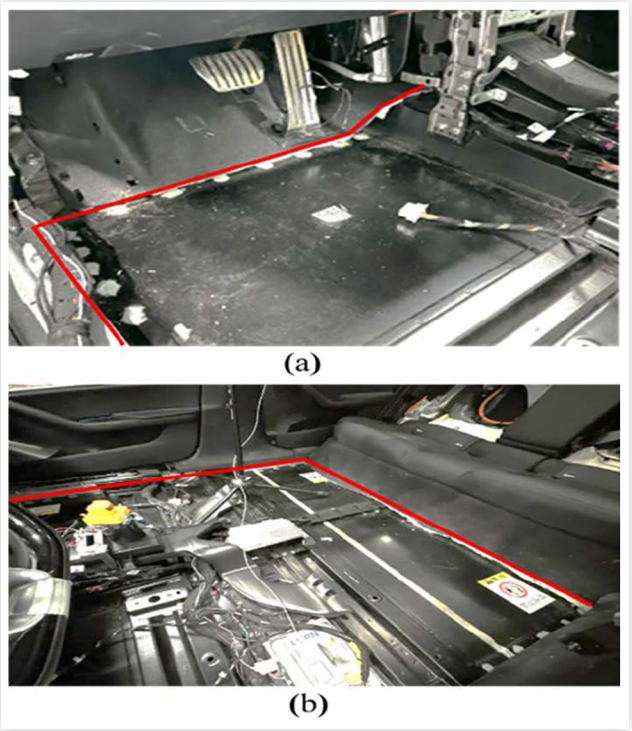

using Siemens Simcenter Testlab. Figures 9 and 10 compare the ATF for front and rear paths between a baseline (original carpet) and a modified configuration (carpet section removed). In the dominant 400–1400 Hz tire noise range [30, 31], a negligible difference is observed across all paths. The specific differences in the 1/3 Octave range of 400–1250 Hz are as follows: 0.36 dB for the front-left tire to the driver's ear (a); 0.01 dB for the front-right tire to the driver's ear (b); 0.58 dB for the rear-left tire to the rear passenger's ear (c); and 0.72 dB for the rear-right tire to the rear passenger's ear (d). This indicates the CTC structure's intrinsic STL is sufficient. Furthermore, this small observed difference may be partly attributed to sound leakage from the material's cut edges—a testing artifact. In production vehicles, a continuous carpet eliminates this leakage path, suggesting the real-world performance difference is even smaller.

In-Vehicle Experiment: Interior Noise

In order to validate the huge advantage of CTC's insulation ability, a practical, in-vehicle comparative assessment was conducted. This approach involved an interior noise test on a smooth asphalt road at a constant speed of 60 km/h. These conditions were chosen to primarily excite tire-road noise while minimizing contributions from wind and the EDU. The comparison was performed between two vehicle configurations: Vehicle A (Baseline): The vehicle with its original, full carpet and insulation pad; Vehicle B (Modified): The same vehicle, but with a section of the

FIGURE 9 Comparison of the ATF performance of different paths: (a) front-left tire to driver's ear; (b) front-right tire to driver's ear.

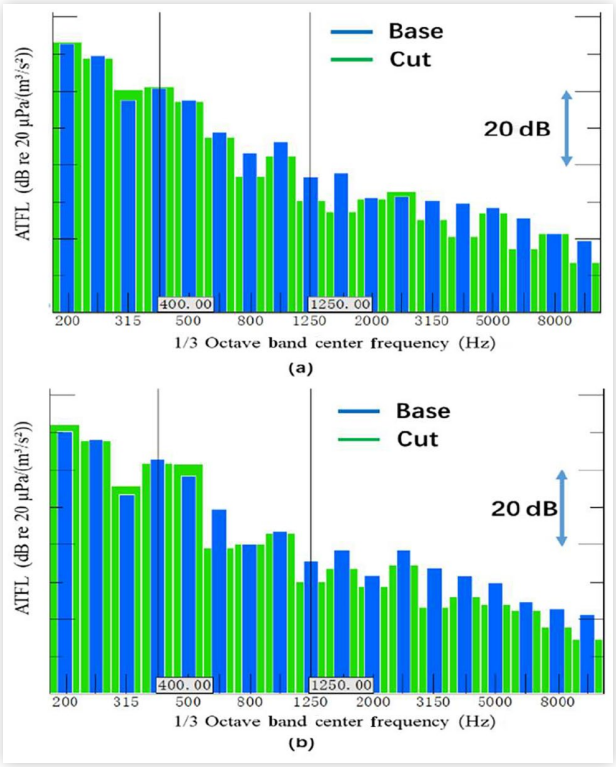

FIGURE 10 Comparison of the ATF performance of different paths: (c) rear-left tire to rear passenger's ear; (d) rear-right tire to rear passenger's ear.

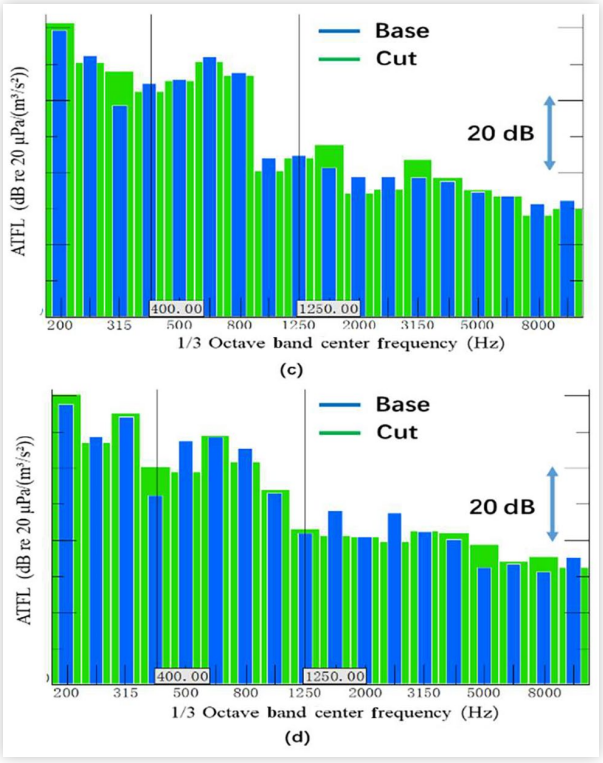

FIGURE 11 Comparison of SPL at the front-left passenger's ear between Vehicle A and Vehicle B at a constant speed of 60 km/h.

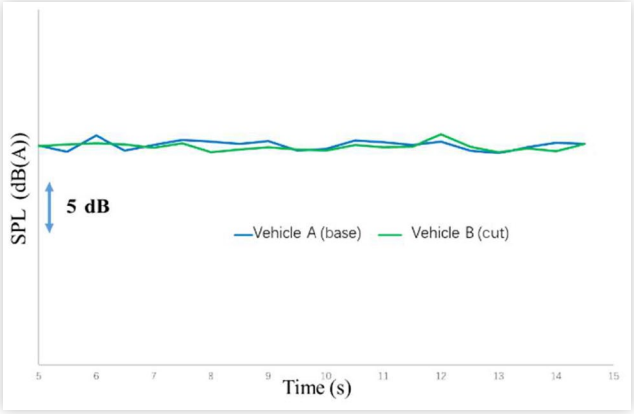

FIGURE 12 Comparison of spectrum at the front-left passenger's ear between Vehicle A and Vehicle B at a constant speed of 60 km/h.

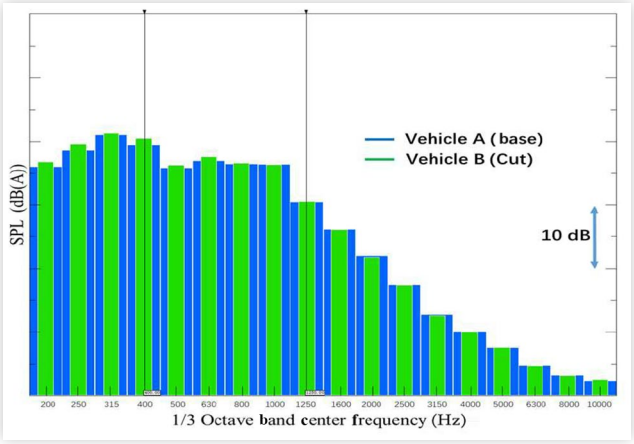

FIGURE 13 Comparison of SPL at the rear-right passenger's ear between Vehicle A and Vehicle B at a constant speed of 60 km/h.

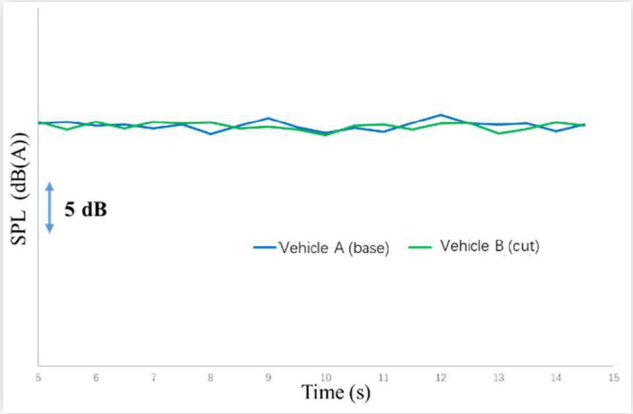

FIGURE 14 Comparison of spectrum at the rear-right passenger's ear between Vehicle A and Vehicle B at a constant speed of 60 km/h.

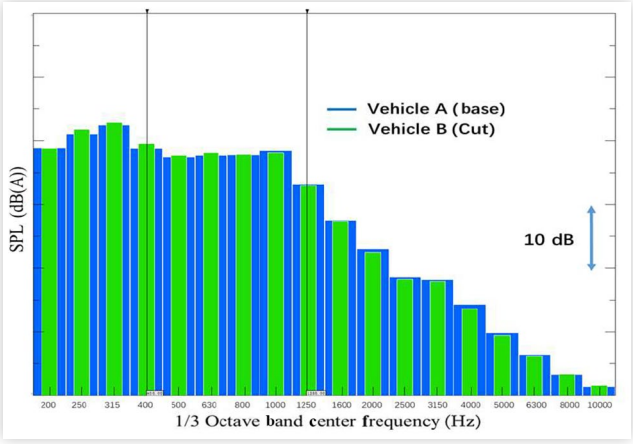

carpet and pad cut. The hypothesis is that if a negligible difference in interior noise is measured between configurations A and B, it would demonstrate that the intrinsic STL of the bare CTC structure is more than sufficient for this application.

Figure 11 plots the overall Sound Pressure Level (SPL) at the driver's ear, showing a negligible average difference of 0.14 dB between Vehicle A (blue line) and Vehicle B (green line). Both curves fluctuate around a similar mean value, influenced by real-world variables such as random wind and road surface profile. Figure 12 shows the spectrum difference of 0.53 dB in the 1/3 Octave frequency range of 400–1250 Hz. Given that both measurements are subject to fluctuations from real-world variables like random wind and road surface profile, this minor difference is considered practically insignificant.

A similar trend is observed at the rear passenger's ear, as shown in Figure 13. Overall, there is no significant average difference (a mere 0.07 dB) in interior noise levels between Vehicle A and Vehicle B in real-world usage. Figure 14 shows the spectrum difference of 0.23 dB in the 1/3 Octave frequency range of 400–1250 Hz. According to the psychoacoustic principle of the Just Noticeable Difference (JND), this value is much smaller than the JND for SPL for the human ear—typically about 1 dB [32]. This indicates that the CTC structure inherently exhibits high STL, so modifications to the carpet and insulation pad have little effect in this specific noise frequency range.

Conclusions

This paper presents a multifaceted investigation into the STL of a novel CTC structure, benchmarked against a conventional floor-CTP system and a traditional ICE single-layer floor. First, a theoretical analysis, based on the mass law and the double-wall principle, was conducted to establish a baseline STL prediction from fundamental physical parameters. Next, to capture complex behaviors beyond the idealized theory, FEA was utilized. These

detailed simulations, incorporating key material properties, successfully identified significant STL dips in the CTC and floor-CTP systems caused by structural resonances and air cavity modes. Finally, the superior STL performance of the CTC structure predicted by the models was experimentally validated through in-vehicle ATF and interior noise measurements. This comprehensive analysis leads to the following key conclusions:

1. Both theoretical analysis and FEA simulations consistently affirm the superior STL performance of the CTC structure. This validates the theoretical approach, based on mass law and double-wall principles, as an effective tool for baseline estimation. Concurrently, FEA proves indispensable for capturing nuanced acoustic behaviors, such as performance dips caused by structural resonances and cavity modes.
2. The CTC structure demonstrates exceptional inherent STL, significantly outperforming both the floor-CTP system and the traditional ICE single-layer floor. This superiority is primarily attributed to its high mass and monolithic design, which functions as a single, formidable sound barrier. In contrast, the analysis also highlights that the STL of the floor-CTP system is critically limited by flanking paths, underscoring the necessity of meticulous
sealing to realize its full double-wall potential.
3. A primary engineering implication is that the CTC structure's high intrinsic STL enables significant optimization of the cabin acoustic package. Specifically, it allows for the downsizing of porous absorbers and the elimination of heavy mass-barrier layers (e.g., EPDM/EVA), creating a direct path to weight and cost reduction. The analysis confirms that for such a high-performance floor, these heavy layers provide diminishing returns. Nevertheless, the sound-absorbing properties of the surface carpet remain valuable for managing high-frequency cabin reverberation, effectively shifting its primary function from sound insulation to sound absorption.

The proposed models have several inherent limitations that should be acknowledged. The analytical model, being rooted in mass-law principles, inherently neglects the structural stiffness of the panels. This simplification restricts its validity to the mass-controlled frequency range, typically between the double-wall resonance and the first air cavity mode. Furthermore, both the analytical and FE models employed idealized boundary conditions, omitting structural flanking paths introduced by bolts and other physical contacts. Consequently, the predicted STL values should be interpreted as an optimistic upper bound, which, as expected, exceeded the performance measured in the vehicle.

This discrepancy highlights a critical challenge in experimental validation: due to the CTC structure's exceptionally high intrinsic STL, the in-vehicle measurements were inevitably dominated by flanking noise transmission through adjacent paths (e.g., firewall, wheel arches, and door glass). This contamination made it impossible to isolate and quantify the true performance of the CTC floor itself. Therefore, future work should prioritize laboratory-based testing using a dedicated transmission loss suite. This controlled environment is essential to eliminate flanking paths and rigorously quantify the remarkable STL potential of the CTC structure revealed in this study.

Contact Information

Xueying Xu
CATL (Shanghai) Intelligent Technology Co., Ltd
beiruzi@126.com

Definitions/Abbreviations

AML - automatically matched layer
ATF - acoustic transfer function
ATFL - acoustic transfer function in level
EDU - electric drive unit
EPDM - ethylene propylene diene monomer
EV - electric vehicle
EVA - ethylene vinyl acetate
FEA - finite element analysis
FL - front left
ICE - internal combustion engine
RR - rear right
SEA - statistic energy analysis
STL - sound transmission loss
VOC - volatile organic compound

References

1. IEA, "Trends in Electric Cars – Global EV Outlook 2024," accessed April 2024, https://www.iea.org/reports/global-ev-outlook-2024/trends-inelectric-cars.
2. Hua, X., Thomas, A., and Shultis, K., "Recent Progress in Battery Electric Vehicle Noise, Vibration, and Harshness," *Science Progress* 104, no. 1 (2021): 368504211005224, doi:https://doi.org/10.1177/00368504211005224.
3. Krüger, C., Spohr, S., Merdivan, D., and Urban, P., "Avoiding Structural Redundancies between the Vehicle Body and the Battery Housing Based on a Functional Integration Approach," *Automotive and Engine Technology* 7, no. 3-4 (2022): 197-208, doi:https://doi.org/10.1007/s41104-022-00106-8.
4. Barathi Raja, K., "Mechanical Design and Packaging Strategies of a Cell-to-Pack Battery for an Automotive Electric Vehicle Based on Economic & Sport Vehicle

Requirements," SAE Technical Paper 2025-28-0078 (2025), doi:https://doi.org/10.4271/2025-28-0078.

5. Xu, X., "Study on Lightweight Development for Acoustic Package Based on Classic Acoustic Theory," *Automobile Technology* 12 (2018): 51-54, doi:https://doi.org/10.19620/j.cnki.1000-3703.20180458.
6. Yoo, T., Gerdes, R., Lee, S., and Shi, T., "A Novel Dissipative Acoustic Material," SAE Technical Paper 2021-01-1128 (2021), doi:https://doi.org/10.4271/2021-01-1128.
7. Fu, Y. and Wang, X., "Advancements and Trends in Vehicle Sound Package for Noise Control: A Comprehensive Review," *Advances in Mechanical Engineering* 17, no. 6 (2025): 16878132251345867, doi:https://doi.org/10.1177/16878132251345867.
8. Brentnall, H., Ronzio, F., Di Marco, F., and Wang, L., "Methods and Solutions for the Integration of the HV Battery into the NVH Development of a BEV," in *Automotive Acoustics Conference 2019*, ed. Siebenpfeiffer, W. (Wiesbaden: Springer Fachmedien Wiesbaden, 2020), 28-46, doi:https://doi.org/10.1007/978-3-658-27669-0_3.
9. Tinnemeyer, J., "Battery Design," in *Electric Vehicle Batteries*, eds. Galyen, B. and Menchaca, F. (Hoboken, NJ: John Wiley & Sons, Ltd, 2025), 53-81, https://doi.org/10.1002/9781394262144.ch3.
10. Czerwinski, F., "Current Trends in Automotive Lightweighting Strategies and Materials," *Materials* 14, no. 21 (2021): 6631, doi:https://doi.org/10.3390/ma14216631.
11. Lian, Y., Ling, H., Jiang, L., Yi, B. et al., "Development of Cell to Body Technology towards High Levels of Integration, High Strength and High Stiffness," SAE Technical Paper 2023-01-0523 (2023), doi:https://doi.org/10.4271/2023-01-0523.
12. Redacted for Review, "Analyzing Effects of Cell to Chassis Technology on Road Noise of Skateboard-Sharing Vehicles," Presented at in *CMAAE 2025*, China, November 7–9, 2025 (in press).
13. Su, J., Li, X., Yang, H., and Wu, T., "Research on Acoustic and Parametric Coupling of Single-Layer Porous Plate – Lightweight Glass Wool Composite Structure Doors for Pure Electric Vehicles," *World Electric Vehicle Journal* 16, no. 7 (2025): 393, doi:https://doi.org/10.3390/wevj16070393.
14. Zhang, Q., Parrett, A., and Wood, M., "Vehicle Dash Mat SEA Modeling and Correlation," SAE Technical Paper 2007-01-2310 (2007), doi:https://doi.org/10.4271/2007-01-2310.
15. Wang, C., "Sound Transmission Loss of an Automotive Floor Panel Section with Cross Members," *Applied Acoustics* 202 (2023): 109177, doi:https://doi.org/10.1016/j.apacoust.2022.109177.
16. Wang, Z., Min, H., Tian, H., Feng, C. et al., "Empirical Prediction of Random Incidence Sound Transmission Loss of Small-Sized Plates from Normal Incidence Measurements," *Journal of Building Engineering* 108 (2025): 112820, doi:https://doi.org/10.1016/j.jobe.2025.112820.
17. Roca, D., "Broadband and Intense Sound Transmission Loss by a Coupled-Resonance Acoustic Metamaterial," *Physical Review Applied* 16, no. 5 (2021): 054018, doi:https://doi.org/10.1103/PhysRevApplied.16.054018.
18. Van Belle, L., Claeys, C., Deckers, E., and Desmet, W., "The Impact of Damping on the Sound Transmission Loss of Locally Resonant Metamaterial Plates," *Journal of Sound and Vibration* 461 (2019): 114909, doi:https://doi.org/10.1016/j.jsv.2019.114909.
19. Patil, A.R. and Goetchius, G.M., "Effect of Damping on Sound Transmission Loss through Automotive Body Panels," SAE Technical Paper 2009-01-2202 (2009), doi:https://doi.org/10.4271/2009-01-2202.
20. Zarastvand, M.R., Ghassabi, M., and Talebitooti, R., "A Review Approach for Sound Propagation Prediction of Plate Constructions," *Archives of Computational Methods in Engineering* 28, no. 4 (2021): 2817-2843, doi:https://doi.org/10.1007/s11831-020-09482-6.
21. Santoni, A., Davy, J.L., Fausti, P., and Bonfiglio, P., "A Review of the Different Approaches to Predict the Sound Transmission Loss of Building Partitions," *Building Acoustics* 27, no. 3 (2020): 253-279, doi:https://doi.org/10.1177/1351010X20911599.
22. Shimizu, T., Toyoda, M., Takahashi, D., and Kawai, Y., "Numerical Analysis of the Influence of Acoustic Resonance in Air Cavities between Windowpanes on Sound Transmission Loss," *Applied Acoustics* 74, no. 8 (2013): 1010-1017, doi:https://doi.org/10.1016/j.apacoust.2012.12.005.
23. Sahu, N.R. and Mandal, B.B., "Development of Tunable Acoustic Materials with Inline Cavity Structure for Enhanced Sound Absorption and Transmission Loss," *Journal of Building Engineering* 82 (2024): 108305, doi:https://doi.org/10.1016/j.jobe.2023.108305.
24. Doutres, O. and Atalla, N., "Acoustic Contributions of a Sound Absorbing Blanket Placed in a Double Panel Structure: Absorption versus Transmission," *Journal of the Acoustical Society of America* 128, no. 2 (2010): 664-671, doi:https://doi.org/10.1121/1.3458845.
25. Legault, J. and Atalla, N., "Numerical and Experimental Investigation of the Effect of Structural Links on the Sound Transmission of a Lightweight Double Panel Structure," *Journal of Sound and Vibration* 324, no. 3 (2009): 712-732, doi:https://doi.org/10.1016/j.jsv.2009.02.019.
26. Nerse, C., Oberst, S., Moore, S., and MacGillivray, I., "Assessment of Flanking Transmissions in Measurements of Sound Transmission Loss of Multi-Layer Panels," Paper presented at in *the 28th International Congress on Sound and Vibration (ICSV28)*, Singapore, July 24–28, 2022.
27. Oyelade, A.O., "Analytical Modelling of Sound Transmission through Finite Clamped Double-Wall

Panels with Magnetic-Linked Stiffness," *Acoustics Australia* 47, no. 2 (2019): 153-163, doi:https://doi.org/10.1007/s40857-019-00156-3.

28. Bies, D.A. and Hansen, C.H., *Engineering Noise Control: Theory and Practice*, 4th ed. (London: CRC Press, 2017), 359-374, doi:https://doi.org/10.1201/9781315273464
29. Siemens AG, "Simcenter Testlab User Manual: Transfer Path Analysis," Siemens Digital Industries Software, accessed July 2024, https://plm.sw.siemens.com/en-US/simcenter/physicaltesting/testlab/.
30. Li, T., "A Review on Physical Mechanisms of Tire-Pavement Interaction Noise," *SAE Int. J. Veh. Dyn., Stab., and NVH* 3, no. 2 (2019): 87-112, doi:https://doi.org/10.4271/10-03-02-0007.
31. Wang, X., *Automotive Tire Noise and Vibrations: Analysis, Measurement and Simulation* (Oxford, UK: Elsevier, 2020), 19-29, ISBN:978-0-12-818409-7
32. Fastl, H. and Zwicker, E., *Psychoacoustics: Facts and Models*, 3rd ed. (Berlin, Heidelberg: Springer, 2007), 175-202, doi:https://doi.org/10.1007/978-3-540-68888-4

ISSN 0148-7191